A. Zanotti, M. Ermacora, G. Campanardi, G. Gibertini
Stereo Particle Image Velocimetry Measurements of Perpendicular Blade-Vortex Interaction over an Oscillating Airfoil
Experiments in Fluids, Vol. 55, N. 9, 2014, 1811 (13 pages)
doi:10.1007/s00348-014-1811-8

Experiments in Fluids manuscript No.
(will be inserted by the editor)

Stereo particle image velocimetry measurements of perpendicular blade-vortex interaction over an oscillating airfoil

A. Zanotti · M. Ermacora · G. Campanardi · G. Gibertini

Received: date / Accepted: date

Abstract The aerodynamic interaction of a stream-wise vortex impacting on a NACA 23012 oscillating airfoil was investigated using stereo particle image velocimetry. The experimental rig enabled the study of the aerodynamic effects due to the blade pitching motion in the interaction with the vortex.

The experimental study focused on the light dynamic stall regime, which represents a typical condition of the retreating blade of a helicopter in forward flight. Particle image velocimetry was applied to a measurement volume close to the airfoil upper surface in order to obtain the three-dimensional interacting flow field. In particular, the experimental results show that during the airfoil downstroke motion, the vortex impact triggers the stall of the local blade section, indicating that detrimental effects on the blade performance can be introduced by perpendicular vortex interactions.

Keywords Stereo PIV · Blade-Vortex Interaction · Oscillating airfoil · Wind Tunnel

A. Zanotti, M. Ermacora, G. Campanardi, G.Gibertini

Politecnico di Milano, Dipartimento di Scienze e Tecnologie Aerospaziali, via La Masa 34, 20156, Milan, Italy

Tel.: +39-02-23998070

E-mail: alex.zanotti@polimi.it

1 Introduction

The aerodynamic interactions between helicopter rotor blades and the vortices produced by the blades themselves exert important and adverse effects on rotor noise (Schmitz and Yu , 1983; Yu , 2000) as well as on rotor performance. Moreover, these aerodynamic interactions cause blade vibrations and instability. Blade-vortex interactions (BVIs) occur mainly when the helicopter is slightly descending (Shockey et al. , 1997) and the tip vortex wake remains in the region of the rotor disk. Depending on the direction of the vortex axis with respect to the blade span, different typical cases of BVI may be considered (Conlisk , 2001; Rockwell , 1998): parallel BVI when the vortex and the blade axes are nominally parallel, perpendicular BVI when the axes are perpendicular and in parallel planes, orthogonal BVI when the axes are in orthogonal planes and oblique BVI when oblique collisions occur between the vortex and the blade.

In parallel BVI, the resulting interaction is highly unsteady, primarily two-dimensional, and distributed over a large span-wise portion of the blade. In contrast, the perpendicular interaction is characterised by a high degree of three-dimensionality as the vortex induces incidence angles anti-symmetrically with respect to its own axis. Other characteristics of a perpendicular interaction are a narrow localisation essentially limited to the extension of the vortex section and a low degree of unsteadiness. Owing to its low unsteadiness, the noise effects of perpendicular BVI are less significant with respect to parallel BVI, as shown by Glegg et al. (1999) and Yu (2000). In parallel BVI, the sudden pressure fluctuations induced by travelling vortices result in the propagation of strong impulsive (harmonic) noise. Subsequent perpendicular BVIs produce a continuous (broadband) noise characterised by a much lower intensity compared to the harmonic noise. Nevertheless, the locally-induced angles of incidence can trigger dynamic stall in the retreating blade and produce rotor vibrations.

The present paper describes an experimental study carried out at Politecnico di Milano that investigated the interacting flow field over an oscillating NACA 23012 airfoil struck by a stream-wise vortex. In particular, the main focus of this study was to demonstrate the changes in the flow field around the blade due to the

vortex interactions and consequently, how they influence blade aerodynamic performance. Experiments reproducing this phenomenon were performed to allow detailed observations and gain physical insight into it. For instance, the experiments conducted by Wittmer et al. (1995); Wittmer and Devenport (1999) investigated the turbulent flow field due to the perpendicular interaction of a stream-wise vortex with a still blade section model. These experimental surveys showed an increase in the extent of the turbulent flow region and in the turbulent intensity due to the interaction of the vortex with the wake of the still blade.

Particle image velocimetry (PIV) was used to provide quantified visualizations of the flow generated during BVIs (Green et al. , 2000; Horner et al. , 1996). The rapid development of this technique has helped gain more detailed insight into the three-dimensional nature of the interacting flow field by using stereo PIV, such as in the experimental study of orthogonal BVI by Green et al. (2006).

Experimental activities (see, for example, Ham (1975); Rife and Devenport (1992); Wittmer et al. (1995); Wittmer and Devenport (1999)) have tipically used a still blade section model struck by a perpendicular vortex without taking into account the target model oscillation. Thus, this important contribution was not considered. The experimental rig employed in this study allowed an investigation of the effects of the blade pitching motion in the study of perpendicular vortex interactions. The stereo PIV technique was used to survey the three-dimensional interacting flow field over the upper surface of the oscillating airfoil at some selected angle of incidence. In particular, the focus of the experiments was to investigate the flow topology of the aerodynamic interaction over a blade section model oscillating in the light dynamic stall regime (Leishman , 2006; McCroskey , 1981). This represents the typical flight condition of the retreating blade of a helicopter in forward flight. Moreover, PIV surveys were also carried out with the target model under steady conditions at the same selected angles of incidence in order to point out the differences between the interacting flow behaviour and the importance of the pitching motion in the study of the BVIs.

2 Experimental method

2.1 Experimental rig set up

The perpendicular BVI tests were carried out at the Aerodynamic Laboratory of the Dipartimento di Scienze e Tecnologie Aerospaziali (DSTA) of Politecnico di Milano. The wind tunnel had a 1 m $\times$ 1.5 m test section. The maximum wind velocity is 55 m/s, and the freestream turbulence level is less than 0.1%. For the present experiment, two airfoil models were used, both with a NACA 23012 section (Leishman , 1990) and a 0.3 m chord length (c). The upstream model spanned half the test section width and was clamped at 10° angle of attack (α). This airfoil model was used as a vortex generator and was mounted on a vertical traversing system in order to adjust the required position of the stream-wise vortex for each test condition.

The second airfoil model represented the target of the impacting vortex and was mechanically jointed with a steel laminae coupling to a driving system that drove the pitch oscillations. The airfoil models were positioned inside the wind tunnel test section so that the leading edge of the oscillating model was 3.5 c past the trailing edge of the vortex generator model. The pitching model was pivoted around the axis at 25% of the airfoil chord. The oscillating model driving system was composed of a brushless servomotor with a 12:1 gear drive. The model pitching motion was controlled by a proportional and a derivative action using an interface software developed in- house in the Labview (Labview User Manual , 1998) environment. A 2048 imp/rev absolute digital encoder with the EnDat 2.2 protocol, directly mounted on the pitching model, was used for feedback control and to provide the trigger signal for the acquisition of the PIV images at the required angle of attack of the target model. Further details on the pitching airfoil experimental rig can be found in Zanotti et al. (2011) and in Zanotti (2012) doctoral dissertation.

Figure 1 shows the schematic layout of the test set up and the reference system used in the present study. The coordinate reference system has the x-axis aligned with the target airfoil chord direction (see Fig. 3) and the origin positioned on the model leading edge.

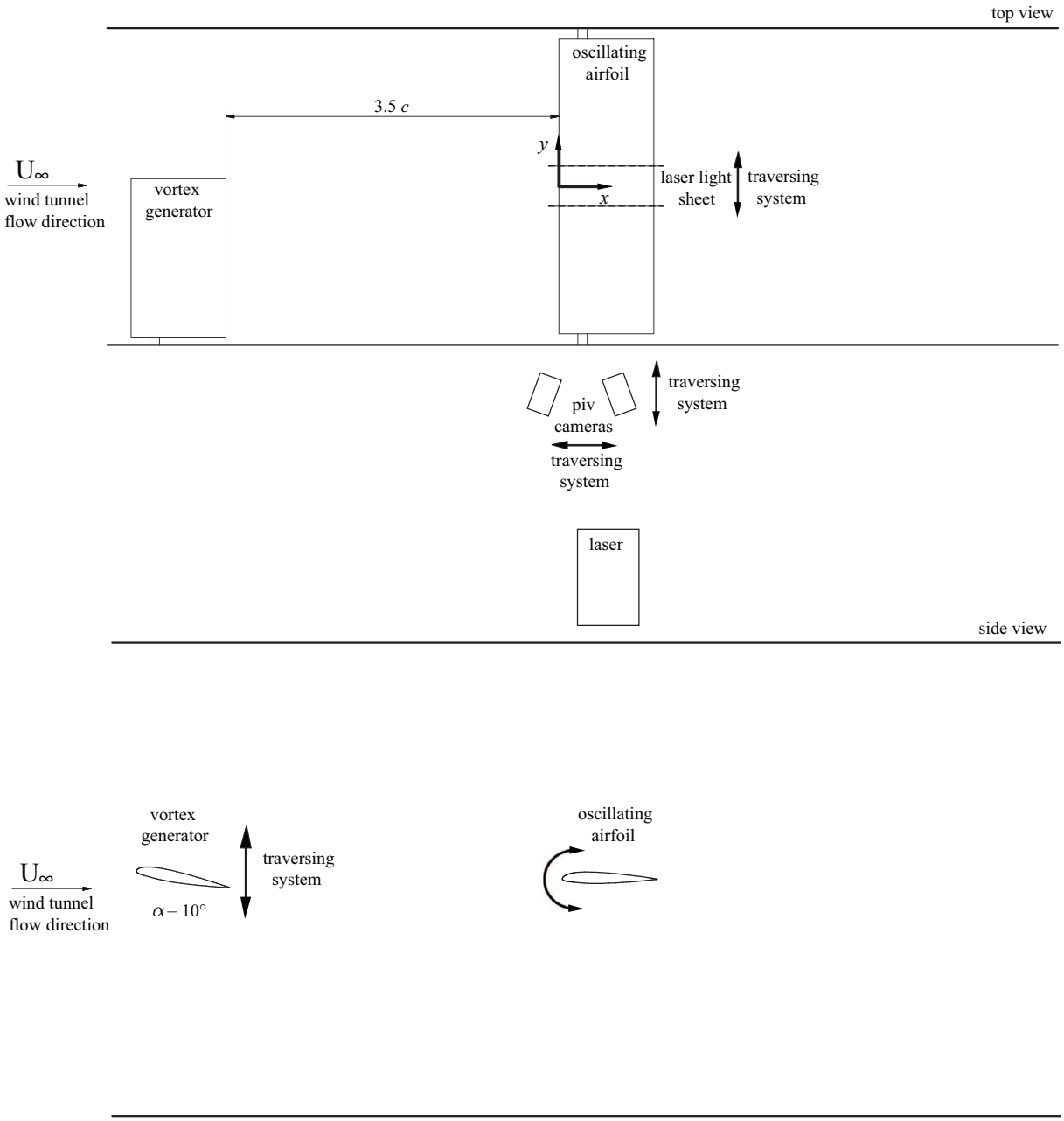

Fig. 1 Schematic layout of the perpendicular BVI test set up. The coordinate system is shown in the top view with z-axis directed out of plane.

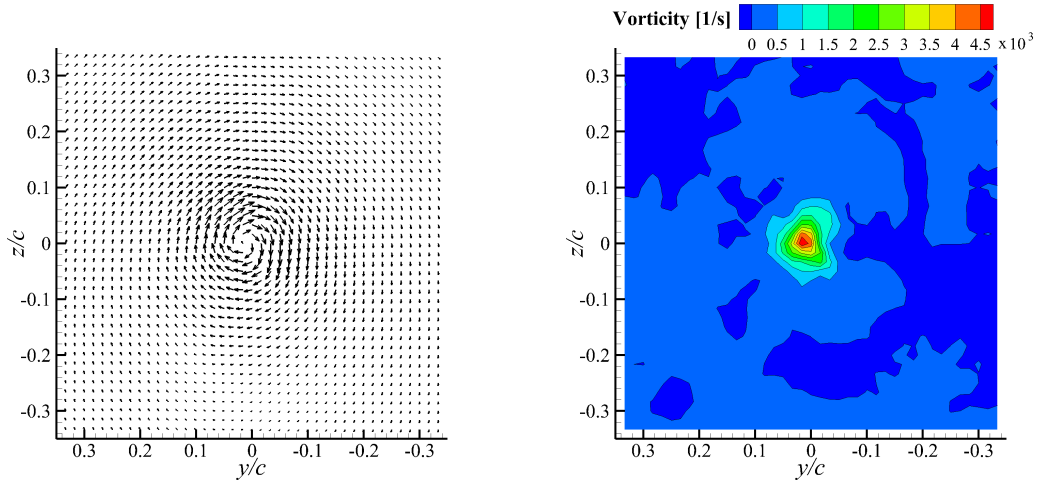

(a) (v,w) velocity field at x/c = 0

(b) vorticity at x/c = 0

Fig. 2 Hot-wire anemometry results for isolated vortex produced by the vortex generator model at $\alpha = 10°$ (Gibertini et al. , 2014): (a) (v,w) velocity field; (b) stream-wise vorticity contours.

A statistical qualification of the isolated vortex was carried out in a previous study (Gibertini et al. , 2014) using three-dimensional hot-wire anemometry. Figure 2 shows the results of the hot-wire measurements carried out on the y-z plane at $x/c = 0$. In particular, the isolated vortex mean velocity field and the stream-wise vorticity contours are presented in Figs. 2a and 2b, respectively. A vortex viscous core radius of approximately 16 mm was evaluated as the radial distance from the vortex core centre of the point with the maximum value of tangential velocity. A problem that affects the stream-wise vortices generated inside a wind-tunnel test chamber is the low-frequency oscillation of the vortex centre-line, called "'vortex wandering"' (Devenport et al. , 1996; Iungo et al. , 2009), that apparently does not affect free-stream vortices. Owing to the wandering, the average vortex is more diffused compared to the actual instantaneous one. The statistical analysis of the hot-wire measurements results demonstrated that in the present experiment, the wandering amplitude is relatively small, with a standard deviation sensibly less than 20% of the vortex core in y- and z- direction (17% and 12%, respectively) (Gibertini et al. , 2014).

In order to investigate wheter the same wandering instability affecting the isolated vortex is present in the interacting test conditions, a statistical analysis was performed of the results of 2C PIV surveys carried out in the region of the target airfoil leading edge on its midspan plane. In particular, the profiles of the vertical velocity component (w) root-mean-square (RMS) were extracted through the vortex core 30 mm ahead of the target airfoil's leading edge. For the test configurations with the target airfoil model at $\alpha = 10^\circ$ and $\alpha = 15^\circ$ in steady conditions, the peak of the w RMS results to be 1.7 m/s and 1.5 m/s, respectively, with a lower value of 1.2 m/s in the isolated vortex configuration at the same longitudinal position. Therefore, even if the differences evaluated between the RMS values are quite small, it can be argued that in the interacting cases, the vortex is oscillating slightly more. This could be due to the flow curvature caused by the target airfoil at incidence or to disturbances coming from the leading edge area.

Owing to the presence of the target airfoil, the vortex core in the proximity of the airfoil leading edge is characterised by a valley in the u velocity profile. An evaluation of the vortex oscillation based on the position of this velocity defect 30 mm ahead of the target airfoil's leading edge produced a result coherent with the results of the w RMS. The vortex position had a standard deviation of 2.7 mm and 2.4 mm at $\alpha = 10^\circ$ and $\alpha = 15^\circ$, respectively, under steady conditions.

2.2 Stereo PIV set up, methodology, and accuracy

The stereo PIV survey over the oscillating airfoil upper surface was set up so that the three velocity components (u,v,w) were measured on x-z plane windows at different span-wise locations for -39 mm $\leq$y$\leq$ 39 mm. The spacing between the measurement planes in the span-wise direction was 3 mm, which is comparable to the dimensions of the interrogation window used for the correlation of the image pairs. The area of investigation was 250 mm $\times$ 47 mm with its lower side at 26 mm from the leading edge (see the sketch in Fig. 3). In order to achieve a higher resolution of the image pairs, the measurement area was composed of two windows with a small overlapping band between them. The PIV system comprised a Litron

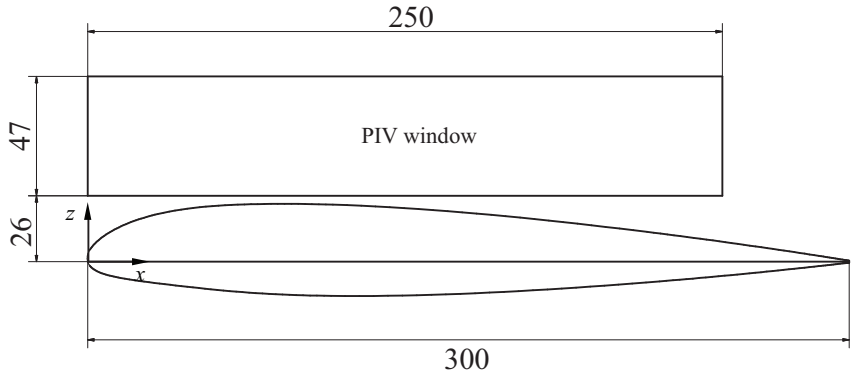

Fig. 3 Sketch of the PIV investigation area on the oscillating airfoil upper surface (dimensions in mm).

NANO-L-200-15 Nd:Yag double pulsed laser with a 200 mJ output energy and a wavelength of 532 nm, and two Imperx ICL-B1921M CCD cameras with a 12 bit, 1952×1112 pixel array. The laser was positioned on top of the wind tunnel test section (see side view in 1). Each camera was equipped with a Nikkor 50 mm lens and tilting type lens for correct focusing of the measurement window. The tilting lens mountings were adjusted in order to achieve the Scheimpflug condition. The camera separation angle could not be higher than 40° owing to the optical access limitation of the wind tunnel test section. The laser and the cameras were connected by a metallic arm and mounted to a double axis traversing system in order to simultaneously move the laser sheet and the measurement window along the oscillating model span-wise and chord-wise directions. The synchronization of the two laser pulses with the image pair exposure was controlled by a 6-channel Quantum Composer QC9618 pulse generator. The signal of the digital encoder mounted on the oscillating model triggered the laser and the cameras with the angle of attack of the oscillating model required for the test every 1/rev. The digital images were captured using a GigaEthernet EBus connection. The calibration of the stereo PIV system was performed using a calibration grid coupled with the oscillating airfoil upper surface in the same position as the laser sheet. A particle generator (PIVpart30 by PIVTEC with Laskin atomizer nozzles) was used for the seeding. The particles consisted of small oil droplets with a diameter in the range of 1-2 μm.

The image pair analysis was carried out by the PIVview 3C software (PIVview User Manual , 2010), developed by PIVTEC in close cooperation with the PIV-Groups of the German Aerospace Center (DLR) in Göttingen and Köln. The first step in the stereo PIV images analysis methodology is the determination of the image back-projection coefficients used to dewarp the images for each camera view. The software also determines the view positions of the cameras using the calibration grid images captured by each camera. The back-projected PIV images pairs are then processed using the two-components (2C) PIV correlation algorithm. In particular, the multigrid interrogation method (Raffel et al. , 2007) was used starting from a 96 pixels $\times$ 96 pixel to a 32 pixel $\times$ 32 pixel interrogation window. The resulting 2C PIV data from both views are then combined to obtain the u,v, and w velocity components using the stereo viewing geometry previously computed. For more details about the stereo PIV analysis methodology, the reader is referred to the PIVview User Manual (2010).

All the resulting velocity fields presented in this paper were phase-averaged over 100 image pairs. This choice was considered a fair compromise between the need to obtain reliable phase averages and an admissible run time. Indeed, owing to the high number of the span-wise measurement planes performed during the experiments, a longer run time required by the PIV measurement might have raised fatigue issues on the model strut. The same number of image pairs was used to perform the phase average of PIV results in the experimental study of parallel BVI carried out by Rival et al. (2010). However, in order to evaluate the statistical convergence, also a phase-average-based on over half the number of the acquired image pairs was also computed and compared with the one based on the full data base. The calculated differences observed on the three velocity components were very small (the maximum value was significantly lower than 1% of the free-stream velocity) for all the considered cases except the ones characterised by a highly chaotic flow (i.e. $\alpha = 15^\circ$ steady and $\alpha = 10^\circ$ downstroke). For these two turbulent cases, differences up to an order of 10% of the free-stream velocity were found in a few data points (less than 1% of the total data set) with an average value on the order of 2% of the free-stream velocity. Thus, the evaluation was repeated for these cases for 75 image pairs, which leads to an halving of the maximum differences. Therefore, the experimental

data-base collected for these test conditions can be considered to illustrate the behaviour of such unsteady flow fields.

The accuracy of the stereo PIV measurements was verified by means of measurements carried out on the isolated vortex without the target model, and compared with three-dimensional hot-wire anemometry measurements for the same test case. The direct comparison of the mean three velocity component profiles evaluated by the hot-wire survey showed a maximum error that was less than 3% of the free-stream velocity (corresponding to an error of about 0.1 px). The accuracy of the present measurements is close to the one found in the Green et al. (2006) experiment for a similar application and in the De Gregorio et al. (2012) stereo PIV surveys carried out on a helicopter model.

2.3 Test conditions

The light dynamic stall cycle (Zanotti et al. , 2013) corresponds to a sinusoidal pitching motion with a mean angle of attack (α_m) of 5°, a constant oscillation amplitude (α_a) of 10°, and a reduced frequency (k) of 0.1. The reduced frequency is defined as $k = \pi f c/U_\infty$, where f is the oscillation frequency, and U_∞ the wind tunnel free-stream velocity. The pitching condition was tested at $U_\infty = 30$ m/s corresponding to a Reynolds number based on airfoil chord of 600 000 and a Mach number of 0.09. This regime is characterised by minor flow separation on the clean airfoil upper surface and consequently a small amount of airload hysteresis, as shown by the lift coefficient curves measured in steady and oscillating conditions presented in Fig. 5 (see Zanotti et al. (2013) for the description of the instrumentation set up).

Some particular phases corresponding to particular incidences in the upstroke or downstroke motion of the airfoil oscillation cycle were chosen to be investigated. For each of these phases, the vortex was made to impact the target model's leading edge region. Thus, a specific test with a specific setting of the upstream wing vertical position was carried out for each considered angle of attack. These same incidences were tested for comparison with the still model as well (steady conditions). Stereo PIV surveys were also performed for

Table 1 PIV test conditions.

Case	α	k	Re	Ma
1	10°	0	$6 \cdot 10^5$	0.09
2	10° upstroke	0.1	$6 \cdot 10^5$	0.09
3	10° downstroke	0.1	$6 \cdot 10^5$	0.09
4	15°	0	$6 \cdot 10^5$	0.09
5	15°	0.1	$6 \cdot 10^5$	0.09

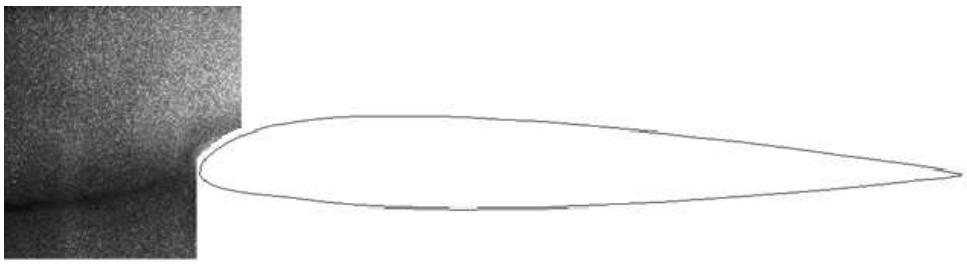

Fig. 4 Particular of the void particle region in a PIV picture used to adjust the position of the vortex generator airfoil. The contrast of the raw image was increased to enhance the void particle region corresponding to the vortex core attitude.

all the test conditions without the impacting vortex in order to clearly evaluate the influence of the blade tip vortex on the flow field. A quite two-dimensional flow behaviour was observed from the results of the tests carried out without vortex interaction.

A summary of the tested incidence angles is presented in Tab. 1. Before the stereo PIV measurements, PIV pictures focusing the target airfoil leading edge region were acquired using one of the cameras with its line of sight perpendicular to the laser sheet. Thus, the vertical position of the vortex generator model was progressively adjusted looking at the void particle region in these preliminary PIV pictures, corresponding to the vortex core attitude (see Fig. 4) (Gibertini et al. , 2014). In the leading edge area, the vortex loses its narrow structure as it is deformed by the presence of the obstacle. Therefore, a quantitative localisation cannot be precisely defined and the impact localisation will therefore be on the order of a few millimetres.

3 Results and discussion

The PIV results are all presented according to the coordinate system illustrated in Figs. 1 and 3. The three-dimensional flow field in the measurement volume was obtained by combining the phase-averaged results obtained from the different span-wise measurement planes.

As shown in Fig. 5, the lift coefficient at $\alpha = 10^\circ$ is essentially the same for the steady case and for the oscillating case in both the upstroke and downstroke motions. Therefore, the choice of this angle of attack allows a comparison between three cases that have the same incidence and the same lift. On the other hand, the test case at $\alpha = 15^\circ$ under dynamic conditions was studied in the present investigation to observe the effect of the impacting vortex when the onset of the lift stall of the airfoil is delayed by the contribution of the oscillation. Owing to the fact that for this angle of attack a comparison of the flow states with the steady case at equal lift was not possible, the three-dimensional flow fields were compared at the same geometric angle of attack in steady and oscillating conditions.

Although the boundary layer separation observed in the present experiments were clearly highly three-dimensional and back-flow is not necessarily associated to three-dimensional separation, the chord-wise velocity component u was taken as a marker of the flow behaviour. In fact, large regions with low u values, particularly when also negative values are present, are a clear indication of stalled conditions. Furthermore, in order to make the vortex structures more visible, vorticity iso-surfaces are presented.

Figure 6 shows the u velocity component contours on y-z planes at different chord-wise locations for $\alpha = 10^\circ$ under steady and oscillating conditions. The figure also includes the flow field measured for the same test cases without the impacting vortex. In order to clearly show the differences of the flow behaviour evaluated with and without the vortex interaction, 3D streamlines are illustrated on the same figure. For greater detail, the u velocity profiles extracted at three different span-wise positions on the same measurement planes are presented in Fig. 7 for the test cases with the impacting vortex, and the iso-surfaces of vorticity magnitude are illustrated in Fig. 8.

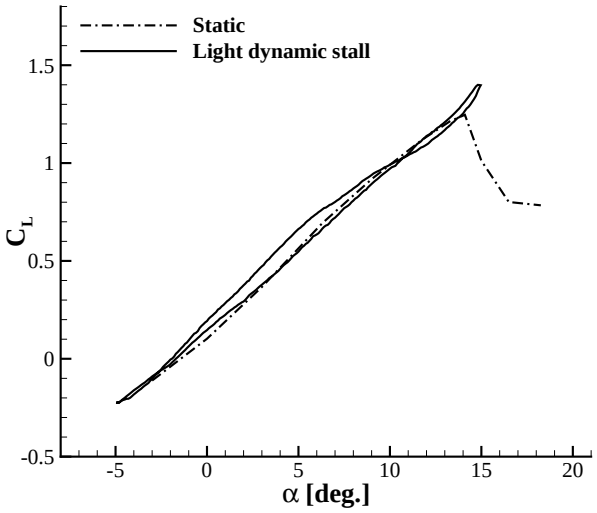

Fig. 5 Comparison of the measured $C_L - \alpha$ curves for the NACA 23012 airfoil in static and light dynamic stall conditions (Re $= 6 \times 10^5$, Ma $= 0.09$).

At this angle of attack, the steady condition is very similar to the corresponding upstroke case. The flow on the airfoil upper surface without vortex interaction is fully attached, as shown by the patterns of the 3D streamlines.

The main effect introduced by the vertical velocity component induced by the vortex is a local variation of the target airfoil angle of attack that is decreased for negative y and increased for positive y. Nevertheless, the measured u velocity profiles do not show back-flow, even in the region when the vortex induces a conspicuous increase of the local angle of attack. In fact, in both these test cases, the vortex remains quite coherent all along the airfoil, as shown in the illustration of the 3D streamlines. The rest of the flow is quite regular and no significant slowdowns are visible. Moreover, it can be observed that the vortex progressively convects towards the positive y direction according to its rotation, which is typical for a vortex close to a wall. The vortex core shift is more clearly visible from the velocity fields plotted at different chord-wise positions in Fig. 9.

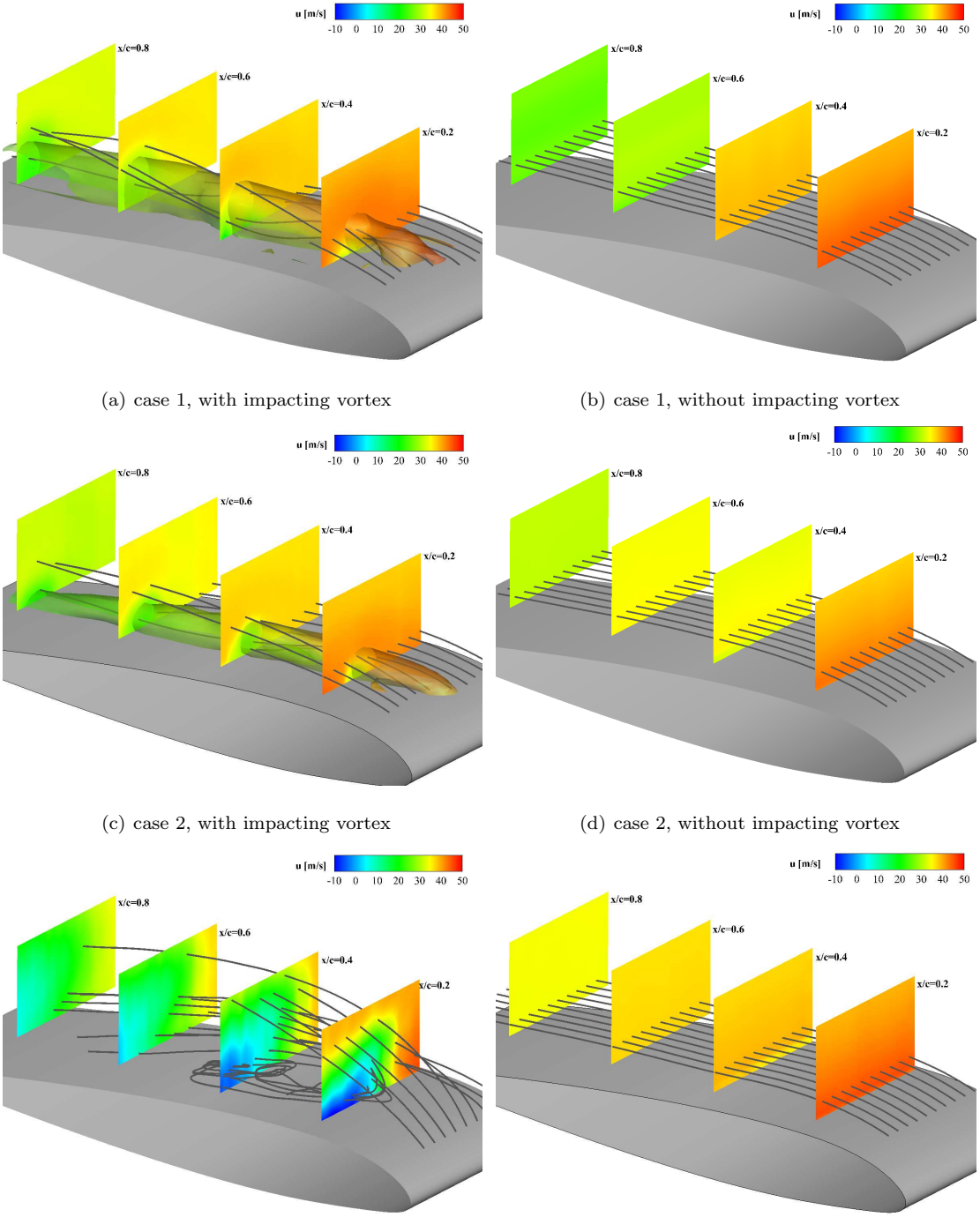

(a) case 1, with impacting vortex

(b) case 1, without impacting vortex

(c) case 2, with impacting vortex

(d) case 2, without impacting vortex

(e) case 3, with impacting vortex

(f) case 3, without impacting vortex

Fig. 6 Stereo PIV results for test cases with the target airfoil at $\alpha = 10°$ in steady and light dynamic stall conditions: u velocity component contours on y-z planes and three-dimensional (3D) streamlines. The iso-surface of the q-criterion coloured by the u velocity component(Hunt et al , 1988) is plotted for the test cases 1 and 2 with the impacting vortex.

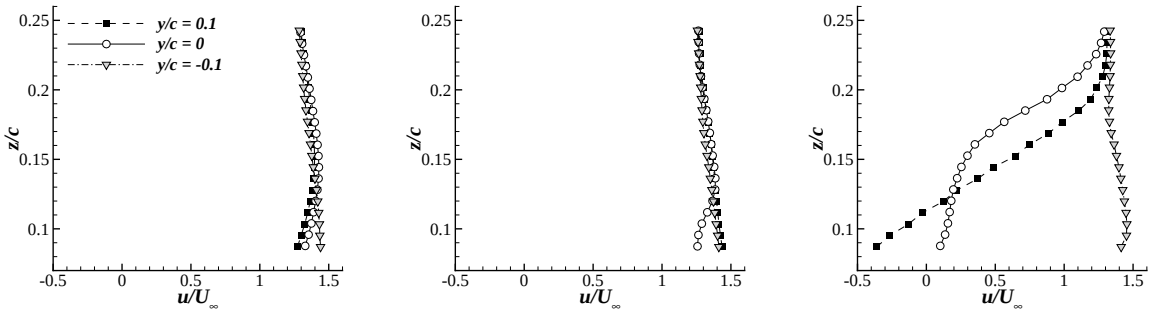

(a) case 1, $x/c = 0.2$ (b) case 2, $x/c = 0.2$ (c) case 3, $x/c = 0.2$

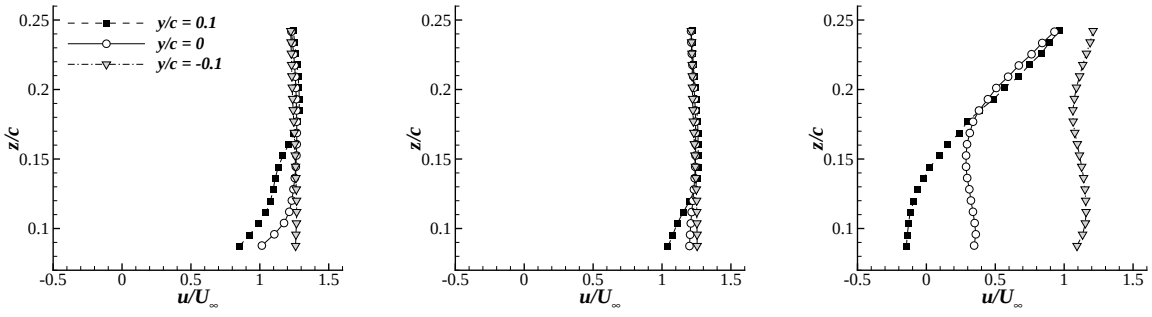

(d) case 1, $x/c = 0.4$ (e) case 2, $x/c = 0.4$ (f) case 3, $x/c = 0.4$

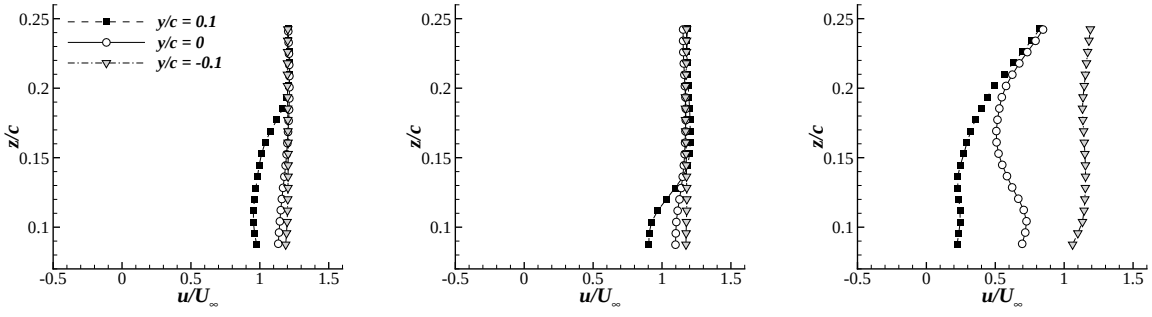

(g) case 1, $x/c = 0.6$ (h) case 2, $x/c = 0.6$ (i) case 3, $x/c = 0.6$

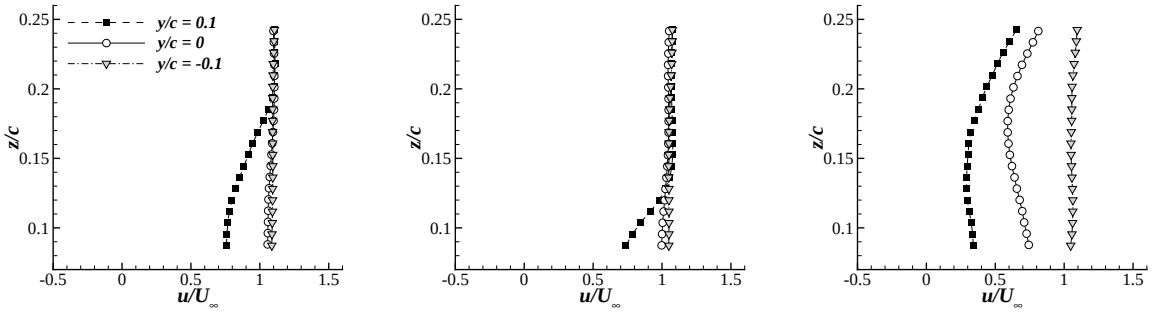

(j) case 1, $x/c = 0.8$ (k) case 2, $x/c = 0.8$ (l) case 3, $x/c = 0.8$

Fig. 7 Stereo PIV results for test cases with the vortex impacting on the target airfoil at $\alpha = 10°$ in steady and light dynamic stall conditions: u velocity component profiles extracted on y-z planes.

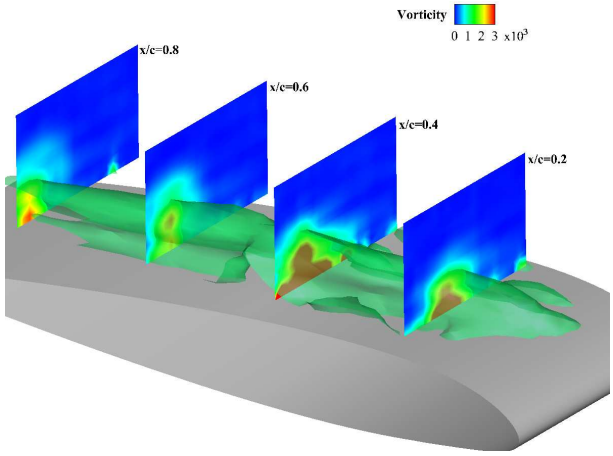

(a) $\alpha = 10°$ steady, case 1

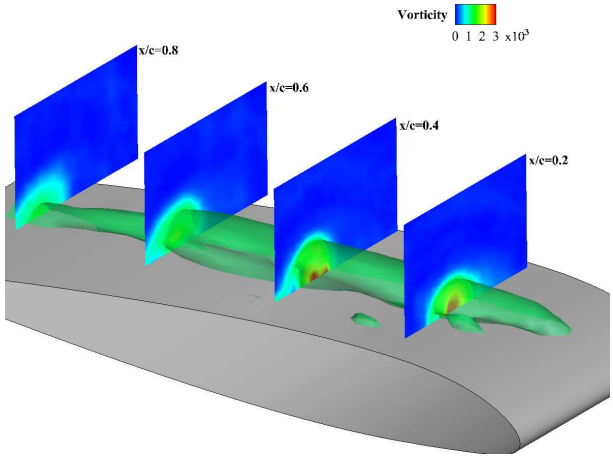

(b) $\alpha = 10°$ upstroke, case 2

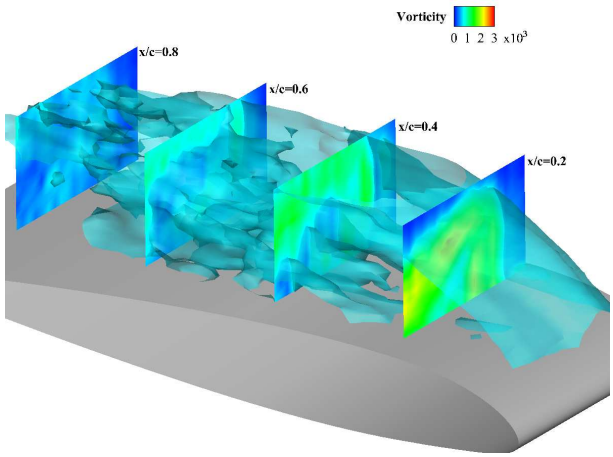

(c) $\alpha = 10°$ downstroke, case 3

Fig. 8 Stereo PIV results for test cases with the vortex impacting on the target airfoil at $\alpha = 10°$ in steady and light dynamic stall conditions: vorticity magnitude contours on y-z planes and iso-surface of vorticity.

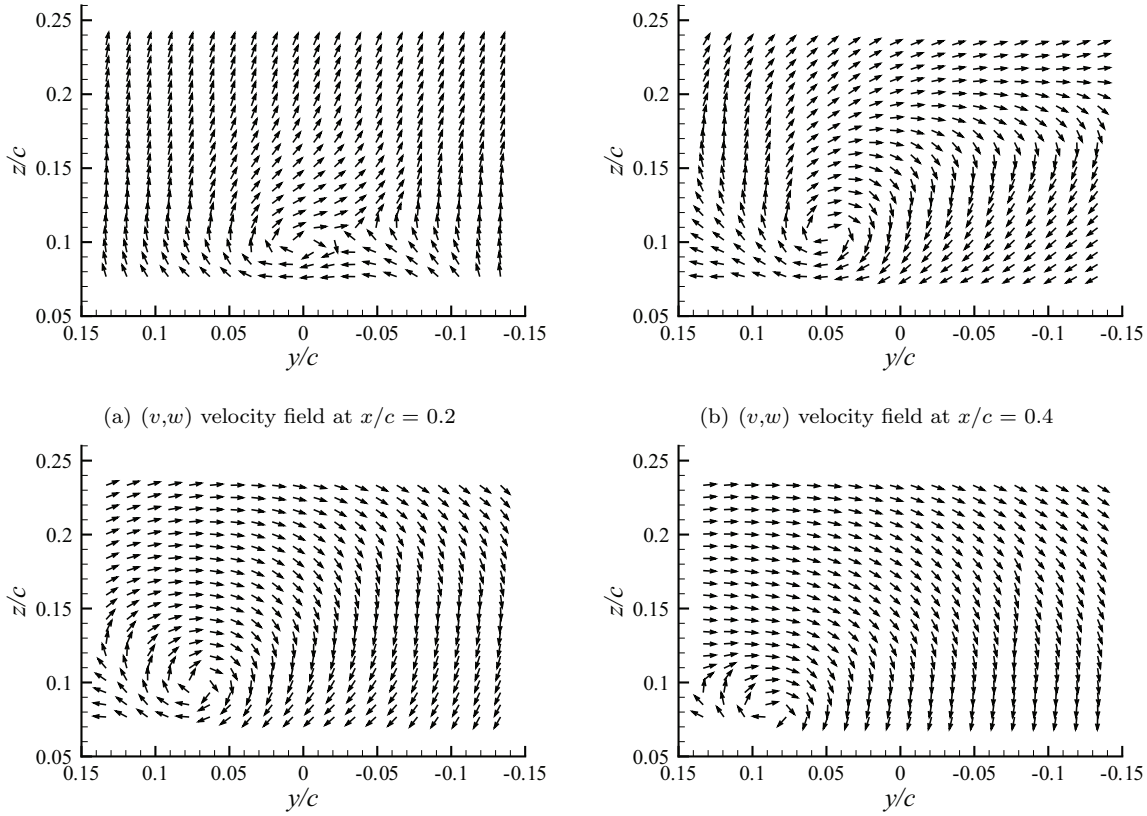

(a) (v,w) velocity field at $x/c = 0.2$

(b) (v,w) velocity field at $x/c = 0.4$

(c) (v,w) velocity field at $x/c = 0.6$

(d) (v,w) velocity field at $x/c = 0.8$

Fig. 9 Stereo PIV results for vortex impacting at $\alpha = 10°$ upstroke under the light dynamic stall condition (case 2): (v,w) velocity fields on y-z planes (vectors are plotted with the same length).

It must be pointed out that this longitudinal vortex structure is not the same vortex impinging on the airfoil leading edge, but it originates from a part of it. In other words, when the vortex arrives at the airfoil leading edge, it is split into a portion flowing below the airfoil and a portion flowing over the upper surface. Therefore, not all the vorticity is convected on the upper region. The vortex locally loses its axi-symmetric structure, and it is strongly diffused owing to the strong local velocity gradients. Nevertheless, the amount of vorticity concentrated in that region collapses again in a vortical structure, although this is characterised by a lower circulation. As shown in Fig. 10, these considerations are supported by the behaviour of the w velocity component profile measured for the interacting case 2 at $x/c = 0.6$ compared to the results

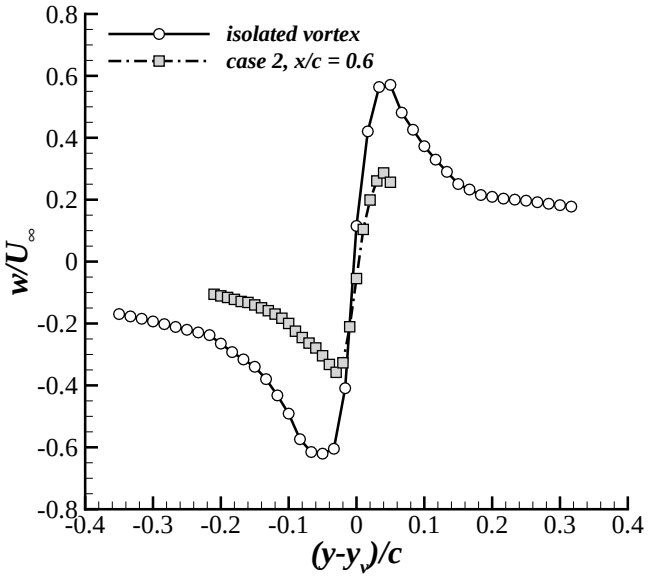

Fig. 10 Comparison of the w velocity component profiles extracted in the span-wise direction in correspondence of the position of the vorticity maximum (y_v,z_v), considered as the vortex centre. Stereo PIV results for the interacting case 2 ($\alpha = 10°$ upstroke) and hot-wire measurements results for isolated vortex case (Gibertini et al. , 2014).

obtained for the isolated vortex case (hot-wire measurements reported in Gibertini et al. (2014)). In fact, the w velocity profile for the interacting case presents a lower peak-to-peak value and a lower slope with respect to the isolated vortex curve.

The test case at $\alpha = 10°$ in downstroke shows the most interesting features of the interacting flow field. As expected for the light dynamic stall condition, the results obtained without the impacting vortex shows a fully attached flow.

For the interacting case, corresponding to the effect of incidence reduction, the u velocity profiles do not show back-flow for negative y. On the other hand, the PIV survey results show a large back-flow region on the airfoil upper surface for positive y where the vortex induces an upward velocity component. In particular, the u velocity profiles extracted at $y/c = 0.1$ show negative values close to the airfoil surface on the planes

at $x/c = 0.2$ and $x/c = 0.4$ (see Fig. 7c and f). The different behaviour of the interacting flow field compared to the case at the same angle of attack in upstroke could be explained by the contributory kinematic effect induced by the rapid negative pitching rate of the airfoil (Leishman , 2006; McCroskey , 1981). This effect, comparable to a modification of the airfoil camber, promotes the local stall onset in this phase of the pitching motion. A quantitative analysis of the influence of the pitching rate can be reasonably achieved under the assumptions of linearised aerodynamics theory. In particular, for the considered light dynamic stall condition, the induced camber effect due to the pitching rate at $\alpha = 10^\circ$ results in a modification of the ideal (Theodorsen) angle of attack of $\pm 1.5^\circ$ (Theodorsen , 1932).

The PIV measurements for the present test case show a certain level of noise compared to the previous test cases owing to the high unsteadiness that characterise the interacting flow field. This feature can be observed from the phase-averaged data that are presented in Fig. 6e, without the application of any kind of smoothing.

An indication of the high chaotic behaviour of this interacting flow field is also highlighted by the iso-surface of vorticity shown in Fig. 8c. In particular, the vorticity magnitude fields on the different y-z planes do not show traces of the coherent vortex structure observed for the test cases at the same angle attack in the steady and upstroke conditions.

The 3D streamlines of Fig. 6e give an intuitive representation of the flow behaviour. A strongly three-dimensional recirculating region is overstepped by the flow coming from the fore region. The internal recirculating flow is related to a spiral node on the airfoil upper surface. A "'finger print"' of this structure can be recognised in the in-plane streamline patterns plotted on the lower face (x-y plane) of the measurement volume (see Fig. 11).

The interacting flow field measured at $\alpha = 15^\circ$ under the steady condition shows a completely different behaviour compared to the one evaluated without the vortex interaction at the same angle of attack. For the interacting case, a wide back-flow region can be observed on the airfoil upper surface that covers almost the entire measurement volume past the airfoil half chord (see Fig. 12a). The behaviour of the u velocity

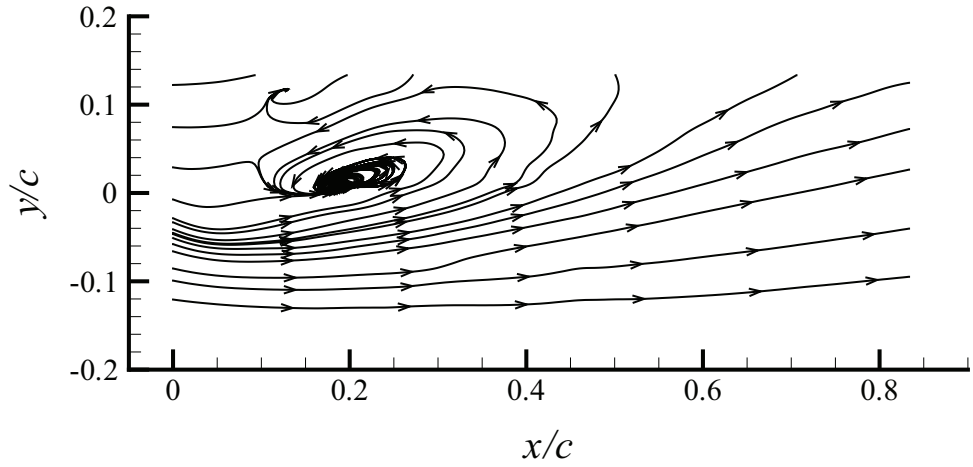

Fig. 11 Stereo PIV results for vortex impacting at $\alpha = 10^\circ$ downstroke in light dynamic stall condition (case 3): in-plane streamlines at $z/c = 0.09$.

component profiles supports this observation (see, in particular, Fig. 13 e and 13g). Corresponding to this flow behaviour, a chaotic flow structure is demonstrated by the iso-surface of vorticity in Fig. 14a. On the other hand, an attached flow behaviour is observed for the corresponding test case without the vortex interaction (see Fig. 12b).

For the same incidence angle of $\alpha = 15^\circ$ in the oscillating condition, the contribution of the oscillation is still capable of delaying the stall onset just as in the case without vortex interaction (see the flow field in Fig. 12d). For the interacting case, analogously to test case 2, the u velocity profiles do not show back-flow, even for positive y where the vortex induces a local increase of angle of attack. The vortex presents a coherent structure that is clearly visible by the 3D streamlines representation and the vorticity magnitude fields shown in Fig. 12c and 14b, respectively. In particular, the vortex clearly presents the same progressive lateral shift effect as that found for the test case at $\alpha = 10^\circ$ in upstroke.

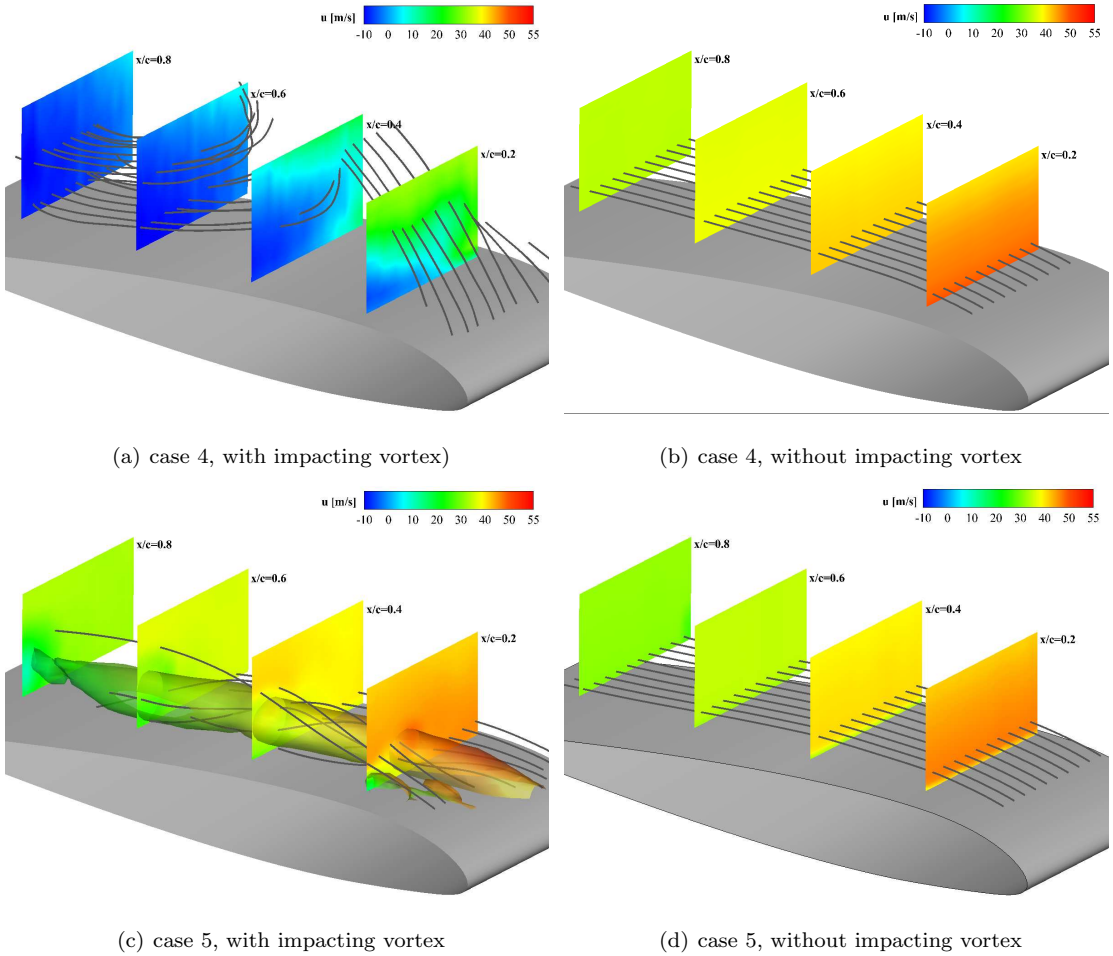

(a) case 4, with impacting vortex)

(b) case 4, without impacting vortex

(c) case 5, with impacting vortex

(d) case 5, without impacting vortex

Fig. 12 Stereo PIV results for test cases with the target airfoil at $\alpha = 15°$ in steady and light dynamic stall conditions: u velocity component contours on y-z planes and 3D streamlines. The iso-surface of the q-criterion coloured by u velocity component(Hunt et al , 1988) is plotted for test case 4 with the impacting vortex.

4 Conclusions

The stereo PIV technique was employed to describe the three-dimensional interacting flow field on the upper surface of an airfoil struck by a perpendicular vortex. The experimental results enabled the comparison of the effects of the impacting vortex over a still and a pitching airfoil. The main goal of the present study of perpendicular BVI problems was to investigate the contribution due to the blade pitching motion during a

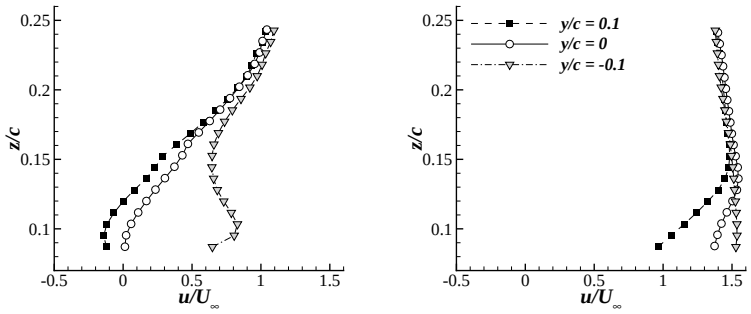

(a) case 4, $x/c = 0.2$ (b) case 5, $x/c = 0.2$

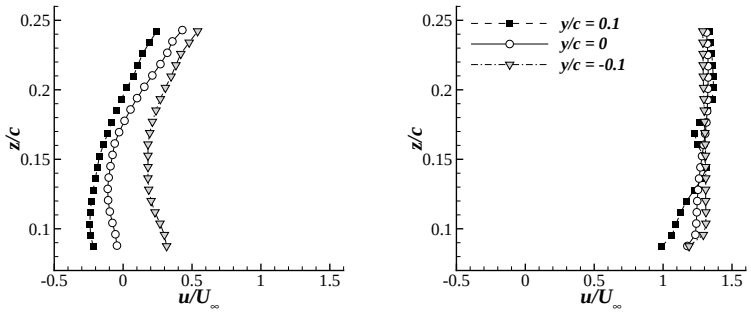

(c) case 4, $x/c = 0.4$ (d) case 5, $x/c = 0.4$

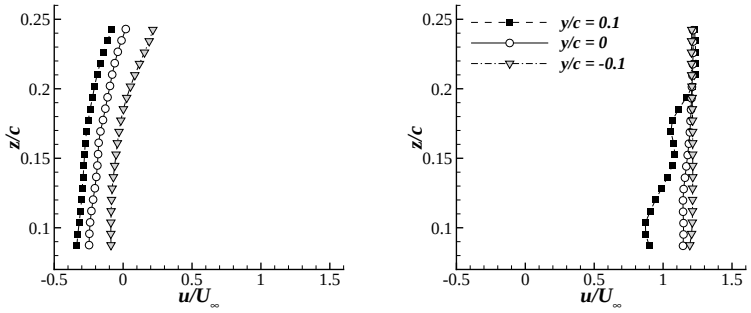

(e) case 4, $x/c = 0.6$ (f) case 5, $x/c = 0.6$

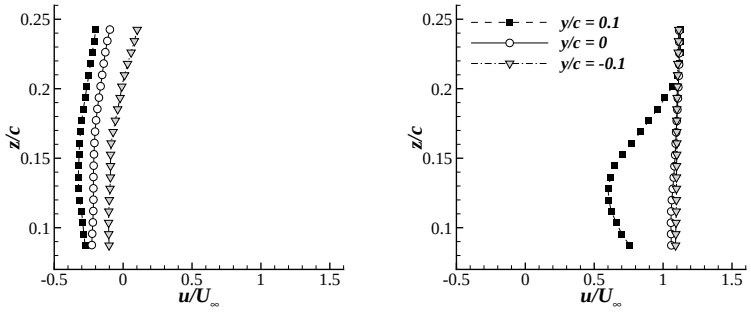

(g) case 4, $x/c = 0.8$ (h) case 5, $x/c = 0.8$

Fig. 13 Stereo PIV results for test cases with vortex impacting on the target airfoil at $\alpha = 15°$ in steady and light dynamic stall conditions: u velocity component profiles extracted on y-z planes.

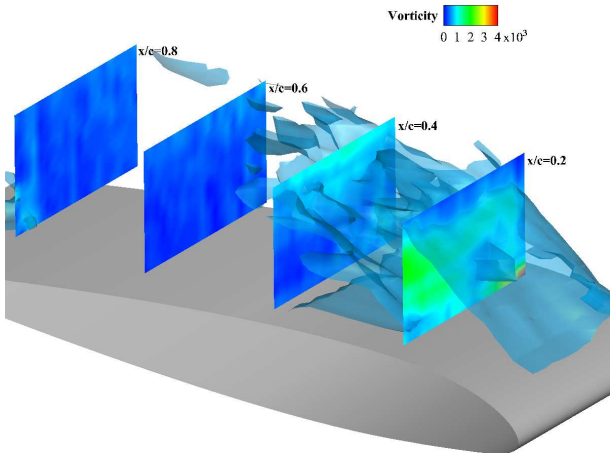

(a) $\alpha = 15°$ steady, case 4

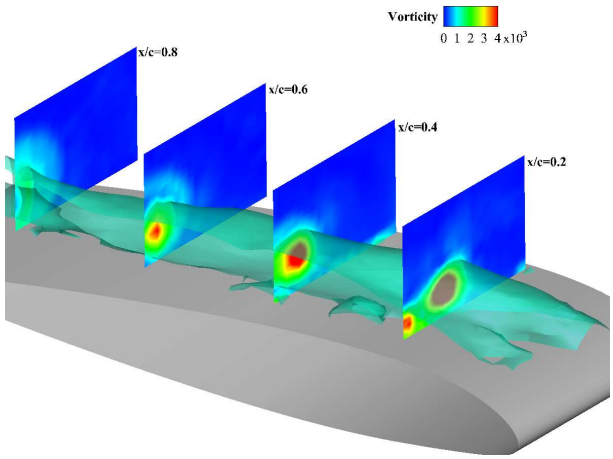

(b) $\alpha = 15°$, case 5

Fig. 14 Stereo PIV results for test cases with vortex impacting on the target airfoil at $\alpha = 15°$ in steady and light dynamic stall conditions: vorticity magnitude contours on y-z planes and iso-surface of vorticity.

rotation cycle. In particular, the experiments were focused on investigating the vortex effects over an airfoil oscillating in the light dynamic stall regime, which represents a typical condition of the retreating blade of a helicopter in forward flight.

The analysis of the stereo PIV results demonstrated that the effects of the impacting vortex on the flow around the target airfoil are significant. The interacting flow field over the oscillating airfoil showed

strong differences between the test cases with the target model at $\alpha = 10^\circ$ in upstroke and downstroke. In particular, a coherent longitudinal vortex was observed on the upper surface region that is related to the impinging vortex structure, although it is characterised by a lower circulation.

In contrast, at the same angle of attack in the downstroke motion, a strong modification of the flow topology was observed. A back-flow region was observed on the airfoil upper surface where the vortex induces an upward velocity component. The different behaviour of the interacting flow observed in this phase of the motion compared to the upstroke is due to the contributory kinematic effect induced by the rapid negative pitching rate. The presented experimental results indicated that perpendicular vortex interactions can also introduce detrimental effects on the blade performance. It was shown that the impinging vortex can trigger local blade stall. This feature can introduce rapid variations of the airload. In particular, the asymmetry of the interacting flow behaviour observed in upstroke and downstroke motion at the same angle of attack indicates that the vortex impact can be responsible for an increase in the airload hysteresis under the dynamic stall condition.

At the top of the pitching motion, $\alpha = 15^\circ$, the interacting flow field on the target airfoil upper surface region reproduces similar features compared to the interacting case at $\alpha = 10^\circ$ in upstroke. The same coherent longitudinal vortex structure was also observed for the interacting case with the target airfoil at $\alpha = 10^\circ$ under the steady condition. On the other hand, the interacting flow field measured with the target model at $\alpha = 15^\circ$ under the steady condition demonstrated a fairly chaotic behaviour characterised by a wide back-flow region. The different topologies of the interacting flow field observed for the test cases at the same angle of attack in steady and oscillating conditions demonstrated the importance of the pitching motion in BVIs.

References

Conlisk A (2001) Modern helicopter rotor aerodynamics. Progress in Aerospace Sciences 37: 419-476.

De Gregorio F, Pengel K and Kindler K (2012) A comprehensive PIV measurement campaign on a fully equipped helicopter model. Experiments in Fluids 53: 37-49.

Devenport W, Rife M, Liapis S. and Follin G (1996) The structure and development of a wing-tip vortex. Journal of Fluid Mechanics 312: 67-106.

Gibertini G, Mencarelli A and Zanotti A (in press) Oscillating Aerofoil and Perpendicular Vortex Interaction. Proceedings of the Institution of Mechanical Engineers, Part G: Journal of Aerospace Engineering 228: 846-858.

Green RB, Doolan C and Cannon R (2000) Measurements of the orthogonal blade-vortex interaction using a particle image velocimetry technique. Experiments in Fluids 29: 369-379.

Green RB, Coton FN and Early JM (2006) On the three-dimensional nature of the orthogonal blade-vortex interaction. Experiments in Fluids 41: 749-761.

Glegg SAL, Devenport WJ, Wittmer KS and Pope DS (1999) Broadband Helicopter Noise Generated by Blade Wake Interactions. Journal of the American Helicopter Society 44: 293-301.

Ham N (1975) Some Conclusions from an Investigation of Blade-Vortex Interaction. Journal of the American Helicopter Society 4: 26-31.

Horner M, Galbraith R, Coton FN, Stewart J and Grant I (1996). Examination of vortex deformation during blade-vortex interaction. AIAA Journal 34: 1188-1194.

Hunt JCR, Wray A. and Moin P (1988) Eddies, stream, and convergence zones in turbulent flows. Center for Turbulence Research Report CTR-S88.

Iungo G, Skinner P, and Buresti G (2009) Correction of wandering smoothing effects on static measurements of a wing-tip vortex. Experiments in Fluids 46: 435-452.

Labview, User Manual, National Instruments, www.ni.com.

Leishman JG (2000) Principles of helicopter aerodynamics, Cambridge University Press.

Leishman JG (1990) Dynamic stall experiments on the NACA 23012 airfoil. Experiments in Fluids 9: 49-58.

McCroskey WJ (1981) The Phenomenon of Dynamic Stall, NASA TM 81264.

PIVview 2C/3C, User Manual, PIVTEC, www.pivtec.com.

Raffel M, Willert C, Wereley S and Kompenhans J (2007) Particle Image Velocimetry - A Practical Guide, Springer Verlag, Berlin.

Raffel M, De Gregorio F, De Groot K, Schneider O, Sheng W, Gibertini G and Seraudie A (2011) On the Generation of a Helicopter Aerodynamic Database. Aeronautical Journal 115: 103-112.

Rife MC and Devenport WJ (1992) Flow Visualizations of Perpendicular Blade Vortex Interactions. NASA CR 192725.

Rival D, Manejev R and Tropea C (2010) Measurement of parallel bladevortex interaction at low Reynolds numbers. Experiments in Fluids 49: 89 -99.Measurement of parallel bladevortex interaction at low Reynolds numbers. Experiments in Fluids 49: 89-99.

Rockwell D (1998) Vortex-body interaction. Annual Review of Fluid Mechanics 30: 199-229.

Schmitz F and Yu Y (1983) Helicopter Impulsive Noise: Theoretical and Experimental Status. NASA TM 84390, Bell Helicopter Textron.

Shockey G, Williamson J and Cox C (1997) AH-1G Helicopter aerodynamic and structural load survey, USAAMRDL TR 76-39, Bell Helicopter Textron.

Theodorsen T (1932) On the theory of wing sections with particular reference to the lift distribution, NACA TR 383.

Wittmer KS, Devenport WJ, Rife MC and Glegg SAL (1995) Perpendicular Blade Vortex Interaction. AIAA Journal 33: 1667-1674.

Wittmer KS and Devenport WJ (1999) Effects of Perpendicular Blade-Vortex Interaction, Part 1: Turbulence Structure and Development. AIAA Journal; 37: 805-812.

Yu Y (2000) Rotor blade-vortex interaction noise, Progress in Aerospace Sciences 36: 97-115.

Zanotti A, Auteri F, Campanardi G and Gibertini G (2011) An Experimental Set Up for the Study of the Retreating Blade Dynamic Stall. 37th European Rotorcraft Forum, Gallarate (VA), Italy, 13-15 September.

Zanotti A (2012) Retreating Blade Dynamic Stall, Ph.D. thesis, Politecnico di Milano.

Zanotti A and Gibertini G (2013) Experimental investigation of the dynamic stall phenomenon on a NACA 23012 oscillating aerofoil. Proceedings of the Institution of Mechanical Engineers, Part G: Journal of Aerospace Engineering 227: 1375-1388.